LBL-34750
UC-406

Lawrence Berkeley Laboratory
UNIVERSITY OF CALIFORNIA

Accelerator & Fusion Research Division

Presented at the NATO Advanced Study Institute, Maratea, Italy, June 28–July 10, 1992, and to be published in the Proceedings

Mirrors for Synchrotron-Radiation Beamlines

M.R. Howells

September 1993

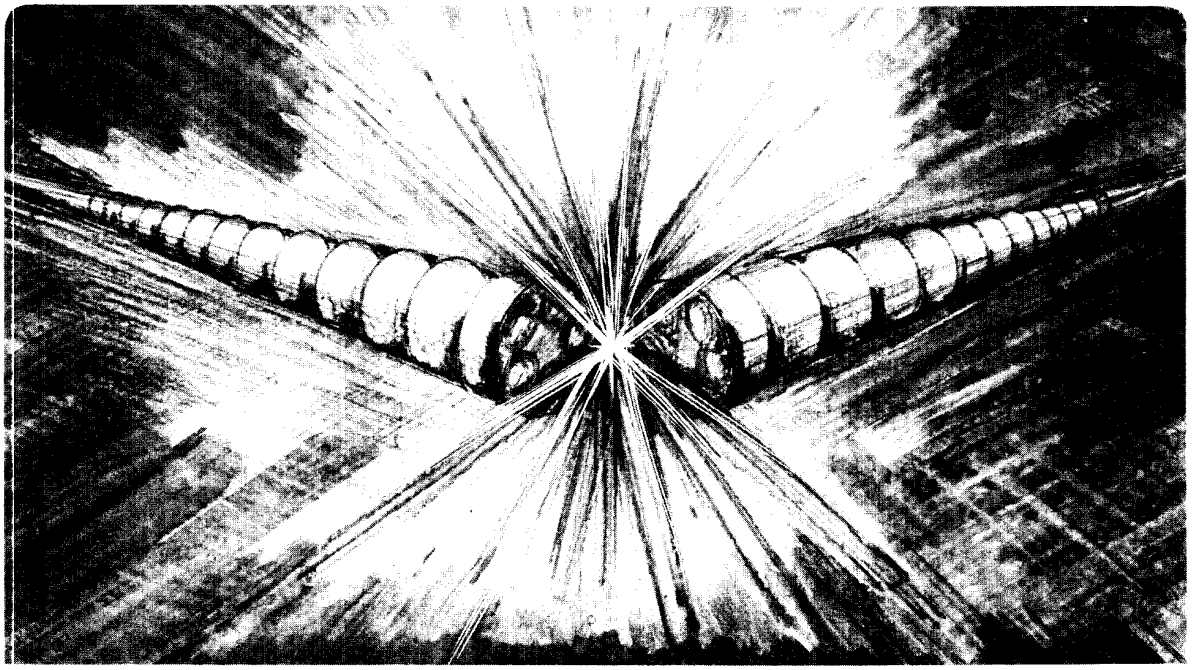

Prepared for the U.S. Department of Energy under Contract Number DE-AC03-76SF00098

LBL-34750
UC-406

Mirrors for Synchrotron-Radiation Beamlines

M.R. Howells
Lawrence Berkeley Laboratory
University of California
Berkeley, California 94720 USA

To be published in the Proceedings of the
NATO Advanced Study Institute

New Directions in Research with Third-Generation Soft X-Ray Synchrotron Radiation Sources

held in Maratea, Italy
June 28–July 10, 1992

Edited by:

A.S. Schlachter
Advanced Light Source
Lawrence Berkeley Laboratory
University of California
Berkeley, California 94720 USA

and

F.J. Wuilleumier
Laboratoire de Spectroscopie
Atomique et Ionique
Université Paris Sud
Orsay, France

This work was supported by the Director, Office of Energy Research, Office of Basic Energy Sciences, Materials Sciences Division, of the U.S. Department of Energy under Contract No. DE-AC03-76SF00098.

MIRRORS FOR SYNCHROTRON-RADIATION BEAMLINES

MALCOLM R. HOWELLS
Advanced Light Source
Lawrence Berkeley Laboratory
Berkeley CA 94720, USA

ABSTRACT. We consider the role of mirrors in synchrotron-radiation beamlines and discuss the optical considerations involved in their design. We discuss toroidal, spherical, elliptical, and paraboloidal mirrors in detail with particular attention to their aberration properties. We give a treatment of the sine condition and describe its role in correcting the coma of axisymmetric systems. We show in detail how coma is inevitable in single-reflection, grazing-incidence systems but correctable in two-reflection systems such as those of the Wolter type. In an appendix, we give the theory of point aberrations of reflectors of a general shape and discuss the question of correct naming of aberrations. In particular, a strict definition of coma is required if attempts at correction are to be based on the sine condition.

1. Introduction

Mirrors are the standard way to manipulate radiation beams at synchrotron-radiation facilities. They are almost always used at grazing incidence, and with the increased sophistication of optical designs and increased power in the radiation beams, they have become an important and challenging branch of optical technology. It is becoming well known that there are important limits to what it is possible to manufacture, so that mirror technology is one of the major limits to the performance of a beamline.

In this paper, we consider the functions of mirrors, the shapes one can conceive, and the standard way to initiate the process of design based on a paraxial analysis. We consider quantitative geometrical descriptions of the important mirror shapes, both in an exact way and by using series expansions. The latter both simplify calculations and make it possible to identify the terms involved in approximating a surface with particular aberrations of the radiation beams reflected from the surface. We study the "sine condition" as a way to understand some of the special limits that apply to single grazing-incidence reflectors and to see the benefits of double-reflection schemes such as the Wolter telescope. Although the benefits of such aberration-canceling schemes are not normally necessary for beamline mirror systems, the same principles apply to grating systems for which aberration canceling can have practical importance. In order to study the aberrations quantitatively, we give a table of some of the terms of the optical-path function expansion in the Appendix, together with a discussion of the naming conventions of the aberrations for systems with and without a symmetry axis. The names must be strictly defined if rules for aberration correction, such as the sine condition, are to be successfully used.

2. Mirrors in Synchrotron-Radiation Beamlines

We show in Table 1 the main functions of mirrors in beamlines and address the important question of whether the optical quality of the mirror limits the spectral resolution of the beamline. Horizontal deflection of the beam is necessary to achieve separation of branch lines derived from the same bending-magnet port. At higher photon energies (smaller grazing angles), such separation can be difficult to achieve, and one must resort to a separation in the distance of the experiments from the source. On the other hand, undulator beams are difficult to split between simultaneous users and are often time-shared. The switching of the beam between the users then involves a mirror or mirrors that can be moved under computer control. This is easier to do nearer the source, such as in switching between monochromators. After the exit slit of a monochromator, the separation achievable with grazing reflections is too small for large experiments like surface-science stations, and the only recourse is to place the experiments on a rotating platform centered at a beamline bellows to act as a "knuckle."

The use of mirrors as energy filters has been practiced since the earliest days of synchrotron radiation-research and has been analyzed, for example, by Rehn (1985). Roughly speaking, the mirror reflects efficiently only for grazing angles smaller than the critical angle $\sqrt{2\delta}$, where δ is the difference from unity of the real part of the refractive index of the mirror coating. The cutoff energy varies by about a factor of 2–2.5 between the

TABLE 1. Functions of beamline mirrors.

Function	Type of mirror (typical)	Resolution determining?	Applications
Deflection	High power, often flat	No	Separation of branches from a port
Energy Filtration	Any	No	Low-pass energy filter, order suppression
Power Absorption	High power, often flat	No	Rejection of power at unwanted photon energies
Condensation	Spherical, toroidal, or ellipsoidal	No	Source to entrance slit (high power), exit slit to sample (low power)
Collimation	High power, spherical, toroidal, or paraboloidal	Yes	Plane grating and crystal monochromators, e.g., to match the beam angular spread to the rocking curve width of a given crystal
Microprobe Formation	Low power, Kirkpatrick-Baez pair, or ellipsoid	Sets *spatial* resolution	Microscopy, fluorescence microanalysis
Focusing	Low power, spherical, toroidal, or paraboloidal	Yes for grating, no for crystal	Plane grating and crystal monochromators

most and the least reflective coatings. The ability of mirrors to carry out this crude filtering is often important for suppressing unwanted high-order diffracted beams from grating monochromators.

In cases where significant power is carried by x rays with energy above the intended range of operation, it is usual to absorb such x rays in the first mirror at grazing incidence. This approach allows subsequent components, which may have a higher grazing angle and may be resolution-determining (with correspondingly tighter tolerances), to operate at lower power load.

Many beamlines have condensing mirrors that either deliver the beam from the source into the entrance slit of a monochromator or relay the beam from the exit slit to the sample. The first type of mirror is normally high power and the second, low power. The surface tolerances are set by the sizes of the object and image in each case, while failure to meet the tolerances leads to a loss of flux and/or spatial resolution but not to a loss of spectral resolution.

The natural vertical opening angle of the synchrotron radiation from the bending magnets of a typical high-energy storage ring is about 5–10 times larger than the rocking curve width of commonly used crystals. Thus there is a motivation to collimate the radiation. Plane diffraction gratings can also profit from a collimation mirror that leads to a wavelength-independent focal position at infinity. Such mirrors are resolution determining.

Finally mirrors may be used for focusing. When they focus the light from a grating to an exit slit, they affect the spectral resolution. When they are used as concentrators for microscopy or microanalysis, they determine the spatial resolution. The most critical cases of the latter occur when the grazing-incidence "forgiveness factor" is not in effect and the (often-multilayer-coated) mirrors are used at *normal* incidence.

3. Paraxial Design: Coddington's Equations

The first step in designing a beamline is the same as for any optical system: paraxial design. This is a preliminary design process that only considers behavior that is second order in the optical path function, that is, focusing effects in the tangential and (separately) in the sagittal plane. Third- and higher-order effects (aberrations) are neglected at this stage. One manifestation of this level of approximation is that the curvatures at every point of an optical surface are approximated by the two principal curvatures at the mirror center (pole). That is, surfaces that have a curvature that varies with position, such as ellipsoids, are effectively approximated as toroids. Even though we shall consider aberrations and the exact shapes of the surfaces later, the paraxial properties, focal lengths, image positions, and so on that we calculate during the paraxial analysis will remain valid. The equations that govern the focusing behavior of a toroid, known as Coddington's equations, thus assume a special importance in beamline design. They are

$$\frac{1}{r}+\frac{1}{r'}=\frac{2}{R\cos\alpha} \qquad \frac{1}{r}+\frac{1}{r'}=\frac{2\cos\alpha}{\rho} \quad , \tag{1}$$

where r is the object distance, r' the image distance, R the major axis, and ρ the minor axis of the toroid. Thus we see that the tangential and sagittal focal lengths, f_t and f_s are given by

$$f_t=\frac{1}{2}R\cos\alpha \qquad f_s=\frac{1}{2}\frac{\rho}{\cos\alpha} \quad , \tag{2}$$

and if one desires that $f_t = f_s$ (stigmatic image), then evidently $r/R = \cos^2\alpha$. These equations can be proved by a geometrical argument (Longhurst, 1962) or by setting F_{200} and F_{020} equal to zero (see Eq. A1 and Table A1).

4. Geometrical Descriptions of Mirror Surfaces

Another useful way to approximate a mirror surface is to express it as a two-dimensional Maclaurin's series with respect to a coordinate system whose y-z plane is the tangent plane at the mirror pole and whose x axis is the normal at the pole. That is

$$x = \sum_{ij} a_{ij} y^i z^j \quad .$$

The coefficients in this series, the a_{ij}'s, are used as descriptors of the mirror surface shape in the aberration series given in the Appendix, which is therefore universal for all mirror shapes. These coefficients are associated with particular point aberrations, and a study of the Maclaurin's series can provide some insight into the nature of the distortions to be expected in wave fronts reflected from a mirror. We give in Tables 2 and 3, the a_{ij}'s for the ellipsoid of revolution and the bicycle-tire toroid which is an arc of the minor radius (ρ) rotated about a point at distance R. From these, one can get the a_{ij}'s of the paraboloid of revolution and

TABLE 2. Ellipsoid of revolution* a_{ij}'s.

i \ j	0	1	2	3	4
0	0	0	$\dfrac{r+r'}{4rr'\cos\alpha}$	0	$a_{02}^3\left(\sin^2\alpha+\dfrac{4rr'\cos^2\alpha}{(r+r')^2}\right)$
1	0	0	$a_{02}\dfrac{\sin\alpha}{2}\left(\dfrac{1}{r}-\dfrac{1}{r'}\right)$	0	*
2	$\dfrac{\cos\alpha(r+r')}{4rr'}$	0	$a_{02}^3\sin^2 2\alpha\left[\dfrac{3}{2}-\dfrac{4rr'}{(r+r')^2}\left(1-\dfrac{\cot^2\alpha}{2}\right)\right]$	0	*
3	$a_{20}\dfrac{\sin\alpha}{2}\left(\dfrac{1}{r}-\dfrac{1}{r'}\right)$	0	*	0	*
4	$a_{20}\left[\dfrac{5\sin^2\alpha}{16}\left(\dfrac{1}{r}-\dfrac{1}{r'}\right)^2+\dfrac{1}{4rr'}\right]$	0	*	0	*

*Paraboloid of revolution a_{ij}'s are obtained from those of the ellipse by setting $r' \to \infty$ for a collimating parabola or $r \to \infty$ for a focusing one, the rays always traveling to the right.

TABLE 3. Bicycle-tire toroid* a_{ij}'s

i \ j	0	1	2	3	4
0	0	0	$\frac{1}{2\rho}$	0	$\frac{1}{8\rho^3}$
1	0	0	0	0	*
2	$\frac{1}{2R}$	0	$\frac{1}{4R^2\rho}$	0	*
3	0	0	*	0	*
4	$\frac{1}{8R^3}$	0	*	0	*

*Apple core toroid a_{ij}'s are the same as those given in this table except for the replacement $R^2\rho \rightarrow R\rho^2$ in a_{22}.

a point at distance R. From these, one can get the a_{ij}'s of the paraboloid of revolution and the apple-core toroid (an arc of radius R rotated about its chord at maximum distance ρ) as explained in the table footnotes. Those of the corresponding cylinders are obtained by setting $j = 0$ and those of the sphere by setting $R = \rho$.

As an example of how useful this representation is, consider the case of an elliptical cylinder mirror such as one might get by bending techniques. The height x of the surface does not depend on z, so we may write it

$$x = a_{20}y^2 + a_{30}y^3 + a_{40}y^4 + \ldots \quad . \tag{3}$$

Hence the curvature is given by

$$\frac{d^2x}{dy^2} = 2a_{20} + 6a_{30}y + 12a_{40}y^2 + \ldots \quad . \tag{4}$$

Suppose the segment of the ellipse is chosen to demagnify the object (Fig. 1). We will then have $r' < r$, so that a_{30} will be negative and the linear term in Eq. (4) will represent a curvature that diminishes with increasing y as it should (Fig. 1). In order to produce an unaberrated image of the axial object point, that is, a circular wave front in the image space, the ellipse needs an a_{30} term of the proper value as given in Table 2. If the mirror were circular instead of elliptical, a_{30} would be zero (according to Table 3), which is larger than the correct (ellipse) value and according to Eq. (3) would cause the wave front to lead the reference sphere when y is positive and lag behind it when y is negative. Alternatively one can also see from Eq. (4) that the change in a_{30} represents an error in the mirror curvature (and hence a similar error in the reflected wave front) that varies linearly with the position, y, in the aperture. This type of twisting of the wave front (which we call aperture defect) moves the outgoing ray in the same direction for all points in the mirror aperture, so that the effect on the image of a point or a line is to produce an asymmetry of the delivered image.

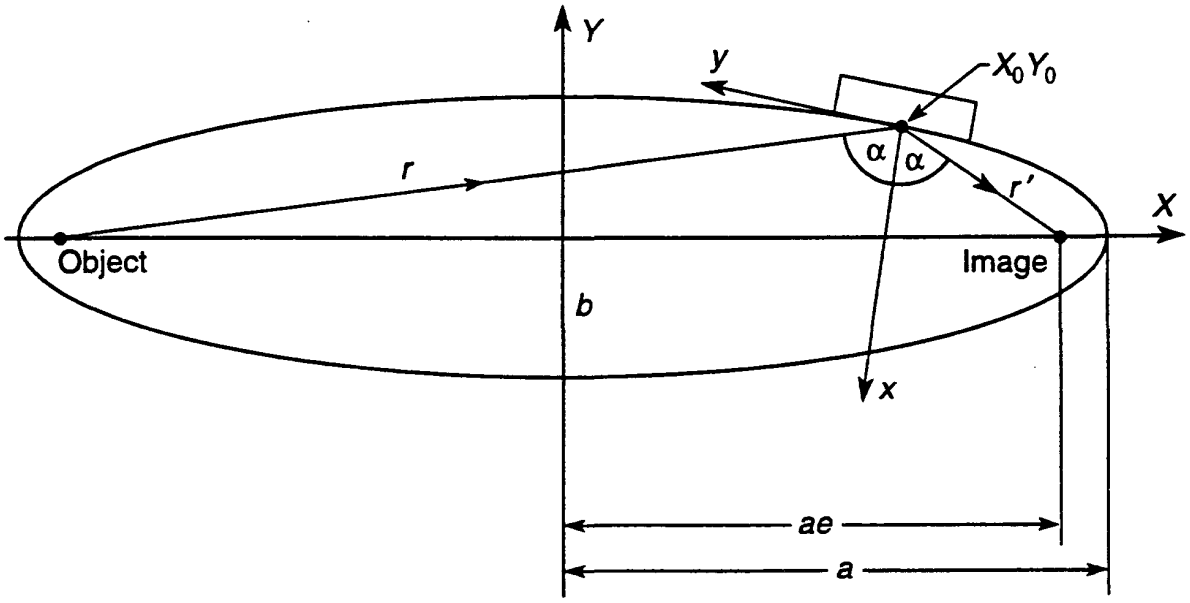

Figure 1. Ellipse geometry and notation.

Similar arguments can elucidate other types of image defect due to other departures of the mirror from the ideal ellipsoid of revolution. It is important to recognize that incorrect a_{ij}'s lead to *point* aberrations (that is, those that do not depend on the z coordinate). Such aberrations can, in principle, always be corrected by altering the shape of the single reflecting surface we are discussing, while those that do depend on z cannot.

5. Toroidal Mirrors

The surface of the bicycle-tire toroid is the easiest aspheric one to fabricate with good figure and finish because it is possible to move the lap in a pseudo-random motion while still maintaining contact with the mirror surface at all points. Thus for toroids (but not for conics), one can use a large lap, which is a great advantage. This leads us to investigate the image quality that can be achieved by using a bicycle-tire toroid mirror, which from now on we will simply call a toroid.

The steep sagittal curvature of the grazing-incidence toroid typically leads to a curvature of the tangential line image, which is the one we would normally like to use to deliver light into a monochromator entrance slit. We will start by evaluating this effect. We are looking for a "$\Delta y' = k\Delta z'^2$ " type of relationship in the image plane [where $(\Delta y', \Delta z')$ are the coordinates of the ray intersection point relative to the Gaussian image point as origin]. We know from applying Eq. (A5) to the astigmatism term (which dominates in determining $\Delta z'$) that

$$\Delta z' = lr'(S+S') \quad , \tag{5}$$

so we need those terms that give a $\Delta y'$ proportional to $\Delta z'^2$, after we take the derivative with respect to w and substitute for l from Eq. (5). There are three such terms as discussed by Welford (1965): F_{102}, F_{111}, and F_{120}. Thus,

$$\Delta y'_{lc} = \frac{r'}{\cos\alpha}\frac{\partial}{\partial w}\left(\frac{1}{2}wl^2F_{120} + wlF_{111} + wF_{102}\right) \quad . \tag{6}$$

Note that none of these terms depends on z (only on z'), so that this is still a point aberration. We consider the case in which the source is a point in the symmetry plane ($z = 0$) and there is some astigmatism. This leads to a type of line curvature named astigmatic curvature by Beutler (1945). There is another type that arises when the source has a finite extent in the z direction (for example, a slit). The latter type comes from F_{102}, with $z \neq 0$ and was named enveloping curvature by Beutler. In practice, both may be present and would be combined as shown in Fig. 2 (Welford, 1965). Returning to Eqs. (5) and (6) and the Appendix, and taking F_{102} and F_{111} from (Noda, 1974), we now have

$$\Delta y'_{lc} = \frac{z'^2\tan\alpha}{2(S+S')^2r'}\left[\frac{S}{r} - \frac{S'}{r'} + \frac{2(S+S')}{r'} - (S+S')^2\right] \quad . \tag{7}$$

Using the above equation for f_s, this becomes

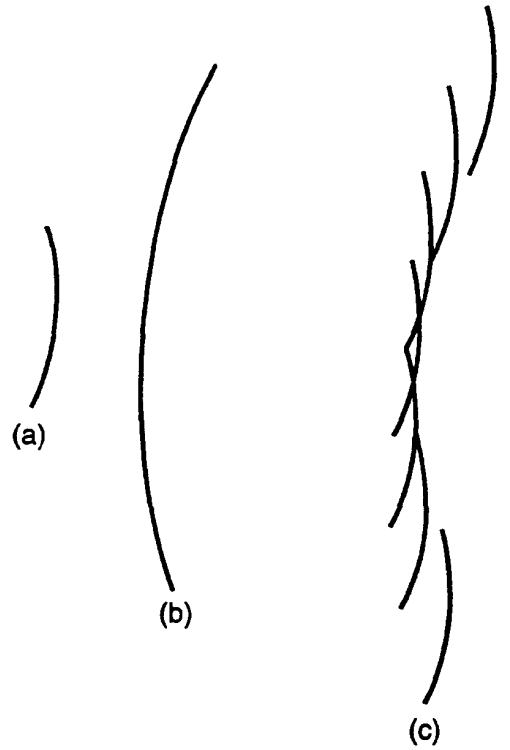

Figure 2. The two types of line curvature. (a) shows the one due to the finite length of the entrance slit, called "enveloping curvature" by Beutler, and (b) shows that of the astigmatic focal line due a point source at the entrance slit, called "astigmatic curvature" by Beutler. In practice the two are combined into a shape formed by displacing either curve along the other as shown in (c). The two effects can have either the same or opposite signs.

$$\Delta y'_{lc} = \frac{l^2 \tan\alpha}{4 f_s}\left[3M + 1 - \frac{2r'}{f_s}\right] \quad , \tag{8}$$

where M (= r/r') is the magnification. This a useful equation for calculating the depth (sag) of the curved line image in the general case where some astigmatism is present ($f_s \neq f_t$). An important special case is the stigmatic image ($f_s = f_t$). Using $f_s = (1/r + 1/r')^{-1}$, Eq. (8) becomes

$$\Delta y'_{lc} = \frac{1}{2}\frac{l^2 \sin\alpha}{\rho}(M-1) \quad . \tag{9}$$

It is noteworthy that the undesirable broadening $\Delta y'_{lc}$, passes through zero for particular choices of the conjugates in both Eq. (8) and Eq. (9). When there is a stigmatic image, the line-curvature aberration is evidently zero for unity magnification. This is sensible intuitively since the mirror surface needed for aberrationless imaging of a point at unity magnification is an ellipsoid with the mirror pole in the symmetric position in the Y-Z plane (Fig. 1). Now the curvatures of an ellipsoidal mirror vary with position on the surface but take stationary (minimum) values in the Y-Z plane. Therefore, a toroid, which has two *constant* curvatures, is a better approximation there than elsewhere. The advantage of unity magnification goes further than eliminating line curvature. It also eliminates the aperture defect (F_{300} aberration), as we discuss below. The good-quality image provided by a toroid at unity magnification has several practical applications in beamline design.

To see the usefulness of Eq. (8) let us define separate magnifications and image distances in the tangential and sagittal planes. Thus $M_t = r'_t/r$ and $M_s = r'_s/r$. Equation (8) now tells us that the curvature of the tangential focal line will be zero provided that

$$M_s = \frac{2M_t}{1+M_t} \quad , \tag{10}$$

so that there is *always* an M_s that gives zero line curvature. This equation is potentially useful also. It is also significant that the line curvature has opposite signs on opposite sides of the magnification value where it passes through zero.

We can derive a useful rule of thumb from Eq. (9) that helps in thinking about possibilities for using toroids in practical situations. Suppose that the radii are chosen for the image to be stigmatic, and the source point is at infinity (M = 0). This is the worst case for using a toroid, being the furthest from unity magnification. At grazing incidence ($\sin\alpha \approx 1$), Eq. (9) reduces to

$$\Delta y'_{lc} \approx \frac{l^2}{2\rho} \quad , \tag{11}$$

which is the *sag* of the toroid in the minor radius direction. This gives a useful "worst-case" feeling for the amount of line curvature to be expected and shows that, in general, the time when a toroid will work best is when it is acting as a weak lens.

We turn now to the next-largest toroid aberration after the line curvature, namely, aperture defect. The ray aberration $\Delta y'_{300}$ is given by

$$\Delta y'_{300} = \frac{r'}{\cos\alpha}\frac{\partial}{\partial w}\left\{\frac{1}{2}w^3 F_{300}\right\} \quad , \tag{12}$$

which leads, in the general case to

$$\Delta y'_{300} = \frac{3}{2} w^2 \left\{ \sin\alpha(M-1) \left[\cos\alpha \left(\frac{1}{r} + \frac{1}{r'} \right) - 2a_{20} \right] - 4r' a_{30} \right\} \quad . \tag{13}$$

Specializing to the case of a toroid for which $a_{30} = 0$ and $a_{20} = 1/2R$ and assuming we are at the tangential focus so that we can apply Coddington's equations, this reduces to

$$\Delta y'_{300} = \frac{3}{2} w^2 \frac{\sin\alpha(M-1)}{R} \quad , \tag{14}$$

or in the common case of grazing incidence ($\sin\alpha \approx 1$) and $M<<1$, we get another useful rule of thumb

$$\Delta y'_{300} \approx \frac{3}{2} \frac{w^2}{R} \quad , \tag{15}$$

which applies equally to spherical and toroidal mirrors since the sagittal properties are not involved. If w is the mirror half-width, then this equation gives the aberration of the marginal ray and is thus a rather pessimistic estimator of image degradation. One can see, for example, that half the rays have aberrations less than one-quarter that of the marginal ray. The aperture defect is the dominant aberration in spherical condensing mirrors such as one would use on an undulator beamline with a monochromator that has an entrance slit. As we noted above, it vanishes at unity magnification or, more generally, it is zero on the Rowland circle.

6. Spherical Mirrors: Kirkpatrick-Baez Systems

The theory given so far for toroidal mirrors applies to spherical ones in the special case $\rho = R$. In view of this, a stigmatic image is not obtainable using a spherical mirror unless $\alpha = 0$. In fact, when spherical mirrors are used at extreme grazing angles (a few degrees or less), the astigmatism is essentially complete. That is, the mirror achieves almost no focusing in the sagittal plane and the rays continue to diverge (or converge) at the same angle as before. At first sight, this appears to be a disadvantage, but in fact it is very useful because one can use a second spherical mirror focusing in the sagittal plane of the first to achieve a focused image in two dimensions as shown in Fig. 3. Such a scheme has less aberration than a single stigmatic toroid at the same grazing angle and is easier to make with good tolerances. It was used in a magnifying microscope configuration in the 1940s and 1950s (Kirkpatrick, 1948), but is now more often used in a demagnifying geometry to form a microprobe (Underwood, 1988) or to condense a beam into a monochromator entrance slit.

Just as toroids are easier than conics to fabricate, so spheres are easier than toroids. The easiest surface of all is a sphere with a loose tolerance on the radius, which is in many ways even easier than a flat. From a fabrication point of view, a flat is like a sphere with a particular value of the radius. The use of spherical optics is now established as the way to get the best figure and finish accuracy. It is often the only way to get optics with the tolerances required to deliver x rays at modern synchrotron radiation facilities without degrading the optical quality of the beam.

The lowest-order aberration is a familiar one from grating theory where it is known that the image of an erect object is formed in a plane steeply inclined to the outgoing principal ray.

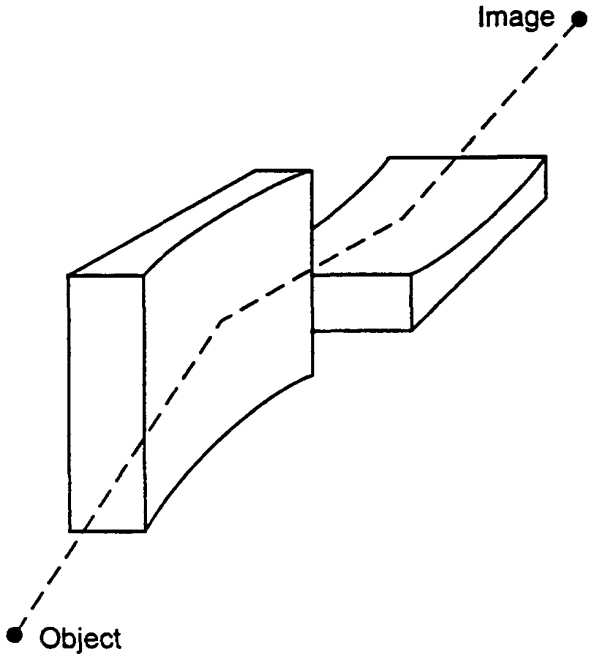

Figure 3. The layout of the two spherical mirrors in the Kirkpatrick-Baez microscope with their tangential planes perpendicular.

One example of such an inclined focal plane is the Rowland circle. This defect, known as obliquity of field, is not represented in the listing in the Appendix because it is a purely in-plane field aberration and there is no field coordinate in the symmetry plane in the Noda description. Nonetheless, the behavior can still be described by considering the focusing condition $F_{200} = 0$ and noting that the tangent of the angle Θ between the focal plane and the principle ray is given by

$$\tan\Theta = r' \left.\frac{\partial\alpha}{\partial r'}\right|_r = \frac{\tan\alpha_G}{M+1} \quad ,$$

where α_G is the grazing angle of incidence. The angle Θ is seen to be always smaller than the grazing angle: obviously a very unfavorable condition for imaging. The difficulty in avoiding the loss of performance caused by this defect was partly responsible for the decline in popularity of the Kirkpatrick-Baez microscope as a device for imaging extended object fields. However, if one only wishes to image a small distant object such as a slit or the synchrotron source, then the defect becomes tolerable and the spherical mirror is very useful. Without the steep curvature of the toroid we now have ρ large and therefore f_s large by Eq. (2) and the line image becomes essentially straight as one would expect [see Eq. (8)] (Hogrefe, *et al.*, 1986). The largest aberration for long-radius spherical mirrors is therefore the aperture defect, which we have already discussed and which is typically the main limit to performance for the spherical condensing mirrors that are now quite widely used. Another limit is the difficulty of making mirrors larger than about one meter long. Current capability does extend up to 1.5 meters but with some worsening in cost, weight, and tolerances for

figure and finish. The consequence of this size limit is that the horizontal collection angles of Kirkpatrick-Baez systems used on bending magnets are rather severely restricted when the photon energy is above a few-hundred eV. However, such systems are well suited to use with undulator beams.

7. Ellipse- and Parabola-Shaped Mirrors

Mirrors shaped as elliptical cylinders and as ellipsoids of revolution are both of interest and have been used on beamlines. For example, both have been used as focusing mirrors for the SX700 plane-grating monochromator (Petersen, 1982; Nyholm, 1986). They are obvious choices for many applications as the two-dimensional and three-dimensional surfaces of exact point-to-point imaging. Paraboloidal cylinders and paraboloids of revolution also have obvious applications and, as we have seen, can often be regarded as a special case of an ellipse with one conjugate equal to infinity. However, it often turns out that these cases are less useful than they might appear. Firstly, the ideal imaging property only applies to the axial object point, and other points are imaged poorly. This is not a fatal disadvantage, and we discuss it further in the section on the sine condition. Secondly, if one puts a full-size lap in contact with any of these surfaces, then the only possible motion of the lap relative to the surface without losing contact is a linear motion in a single direction for the cylinders and rotation in a single direction for the surfaces of revolution. This is not sufficient for good polishing, so one must have recourse to zone polishing using a small or a flexible lap. Such an approach gives much worse errors in figure and finish and with greater effort and cost than using a large lap. The result is that it is hard to get good-quality mirrors in this category. The ellipsoidal mirrors in the SX700s have always been the limiting component of those systems, and their manufacturing tolerances determined the achievable spectral resolution. The plane-grating monochromators at the National Synchrotron Light Source were similarly limited in resolution by the fabrication tolerances of their parabolic mirrors. The most promising strategy for obtaining an ellipse of high accuracy, in this author's opinion, is to use bending, which is only applicable for an elliptical cylinder but does allow the surface to be manufactured as a flat. Diamond turning is an acceptable way to *generate* the surfaces of revolution, but the polishing problem described above still remains.

First consider an elliptical mirror whose action is defined by the object and image conjugates r and r' and the included angle 2α (see Fig. 1). The equation of the ellipse is $X^2/a^2 + Y^2/b^2 = 1$ where a and b are the semi-major and semi-minor axes, respectively. The ellipse parameters a, b and the eccentricity e can be expressed in terms of the user-specified quantities r, r' and α by means of the focus-directrix definition of the shape of the ellipse and the geometry of Fig. 2:

$$\begin{aligned} 2a &= r + r' \\ (2ae)^2 &= r^2 + r'^2 - 2rr'\cos 2\alpha \\ b^2 &= a^2\left(1 - e^2\right) \quad . \end{aligned} \tag{16}$$

The coordinates of the pole of the mirror are

$$X_0 = \pm a\sqrt{1 - \frac{Y_0^2}{b^2}} \qquad Y_0 = \frac{rr'\sin 2\alpha}{2ae} \quad , \tag{17}$$

where the square root is +, 0, or −, depending on whether r is greater than, equal to, or less than r'. The tangential radius of curvature R_p at the pole of the mirror is given by

$$R_p = \frac{(rr')^{3/2}}{ab} \quad , \tag{18}$$

and the angle δ between the tangent at the mirror pole and the x axis is given by

$$\delta = \cos^{-1}\left(\frac{\sin\alpha}{e}\right) \quad . \tag{19}$$

For a parabola, defined by the focal length r and included angle 2α, the equation is $Y^2 = 4a_0X$, where a_0 is the semi-latus rectum. The latter is given by

$$a_0 = r\cos^2\alpha \tag{20}$$

while the pole of the mirror is the point

$$X_0 = a_0\tan^2\alpha \qquad Y_0 = 2a_0\tan\alpha \quad . \tag{21}$$

R_p is given by

$$R_p = \frac{2a_0}{\cos^3\alpha} \quad , \tag{22}$$

and the angle δ between the tangent at the mirror pole and the x axis is $\cot^{-1}\alpha$. R_p is useful for paraxial design, and δ for making coordinate transforms between the X-Y and x-y systems.

The applications of conic mirrors that one encounters in synchrotron practice are usually quite unsophisticated, and one has little need to understand the geometry in a serious way. For applications in which a high-resolution *image* is required, as opposed to reproduction of a simple shape, this situation changes and one needs to understand the behavior of the wave fronts in a more complete way. In such cases, the reader is referred to one of the treatments in the literature that deal with conic and similar mirrors at a deeper level (Brueggemann, 1968; Cornbleet, 1984; Korsch, 1991).

8. The Sine Condition and Coma in Axisymmetric Grazing-Incidence Mirrors

8.1. GENERAL ARGUMENTS

We turn now to the role of the sine condition in determining the aberrations of grazing incidence systems with an axis of symmetry. The sine condition (Abbe, 1879; Welford, 1962, 1976) states that for all rays one must have

$$\frac{\sin\phi}{\sin\phi'} = \frac{\phi_p}{\phi_p'} \quad , \tag{23}$$

where ϕ and ϕ' are the angles of the inward and outward rays to the symmetry axis and ϕ_p and ϕ'_p are the same thing in the paraxial regime. Satisfying the condition guarantees that a system free of spherical aberration is also free of coma. The coma involved in this theorem is strictly the aberration of the axisymmetric system, which depends linearly on the field angle measured from the symmetry axis and is defined, for example, by Born and Wolf (1980). As pointed out by Underwood (1992), the aberrations of grazing-incidence systems with only a *plane* of symmetry (which have been loosely called coma by some workers) cannot be corrected by obeying the sine condition or any derivative of it. The proper naming of aberrations is discussed further in the Appendix. Here we only emphasize again that since the aberrations of greatest interest to us—line curvature and aperture defect—are not really coma, they are not corrected by obeying the sine condition.

Of course, there are grazing-incidence systems that do have a symmetry axis. Such systems are widely used in x-ray telescopes. The main ideas on which they are based were first described by Wolter in a landmark paper in 1952, long before the technology needed to implement the ideas effectively became available. We give a distillation of these ideas in what follows and discuss the possibility of applications to synchrotron-radiation systems.

The first important idea can be expressed as follows. Given object and image points O and I lying on the axis and distant u and v, respectively, from the center A of the system (Fig. 4), construct a new point, B, such that A and B are harmonic conjugates with respect to O and I. That means that B divides OI externally in the same ratio that A divides it internally. Draw a sphere with AB as diameter. It can be shown that the sine condition is equivalent to the requirement that the locus of the intersection points P of the inward rays from O and the corresponding outward rays to I should be the sphere AB. This locus, called the

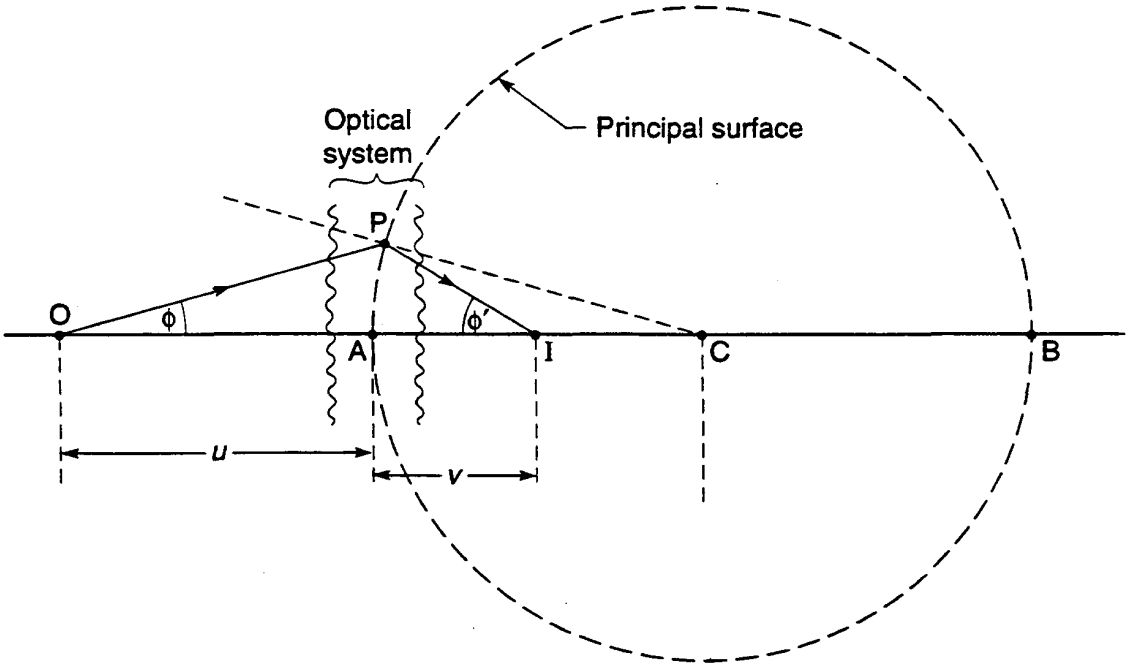

Figure 4. The geometrical form of the sine condition. Let A and B be harmonic conjugates with respect to the object and image points O and I. Draw a circle on AB as diameter. The requirement that the locus of the ray intersection point P be the circle AB is equivalent to the sine condition.

"Kniefläche" by Wolter, is usually translated "principal surface" in English. From the point of view of grazing-incidence systems, which generally have small deflection angles, the *plane* through A normal to the axis will be a reasonable approximation to the sphere.

Suppose now that we have a segment of a single grazing-incidence ellipsoid of revolution with object and image points at the foci of the ellipse (Fig. 5a). We immediately see that the principal surface in this case is the surface of the mirror itself, and it is roughly *perpendicular* to the spherical surface that it would need to be to obey the sine condition (Underwood, 1978). It is obvious from this that any single-reflection grazing-incidence mirror violates the sine condition grossly and can never be coma-corrected. On the other hand, consider a different segment of the ellipse (Fig. 5b) again operating with the object and image points at the foci but this time in *normal incidence*. In this case, the principal surface is still the mirror itself, but now it closely approximates the spherical surface required to satisfy the sine condition. A high degree of coma correction is therefore expected. One way to achieve a similarly high degree of coma correction in a grazing-incidence system is to use a double reflection as in the Wolter telescope and microscope systems (Fig. 5c). Variants of these have been widely used in recent years, particularly as x-ray telescopes. In the next section, we give plausibility arguments showing how coma is produced and how the double-reflection principle can be used to correct it.

8.2. CALCULATION OF THE COMA CIRCLE

First consider a paraboloid of revolution being used to focus parallel light (Fig. 6) and consider the image formed by a thin ring of reflecting surface $P_1P_2P_3$. For the rays that enter parallel to the axis, shown as thin lines, the image is perfect and the rays unite at the focus F. Thus, there is no spherical aberration. For the rays (shown dashed) that enter at a small angle δ below the axis-parallel ones, the reflected rays from P_1 and P_3 will both be deflected downward and will meet the focal plane at F_2 and F_3, which are both below F. In the projection, in which the ray is seen through P_2, it appears undeflected and arrives at F_2, which is above F. From the geometry of the figure we can see that

$$FF_1 = \frac{-r' \sin \delta}{\cos(\psi + \delta)} \qquad FF_3 = \frac{-r' \sin \delta}{\cos(\psi - \delta)} \qquad FF_2 = r' \tan \delta \quad , \tag{24}$$

where $r' = P_1F$ and the angle $2\psi = P_1FP_3$. If we now take $\delta << \psi$, F_1 and F_3 become the same, and both have

$$y = \frac{-r'\delta}{\cos \psi} \quad , \tag{25}$$

while F_2 has

$$y = r'\delta \quad . \tag{26}$$

By considering other reflection points on the ring $P_1P_2P_3$, we can see that, for the rays inclined to the axis by δ, the image will be a circle centered on F, and, from (25) and (26), the radius of the circle R_c must be given by

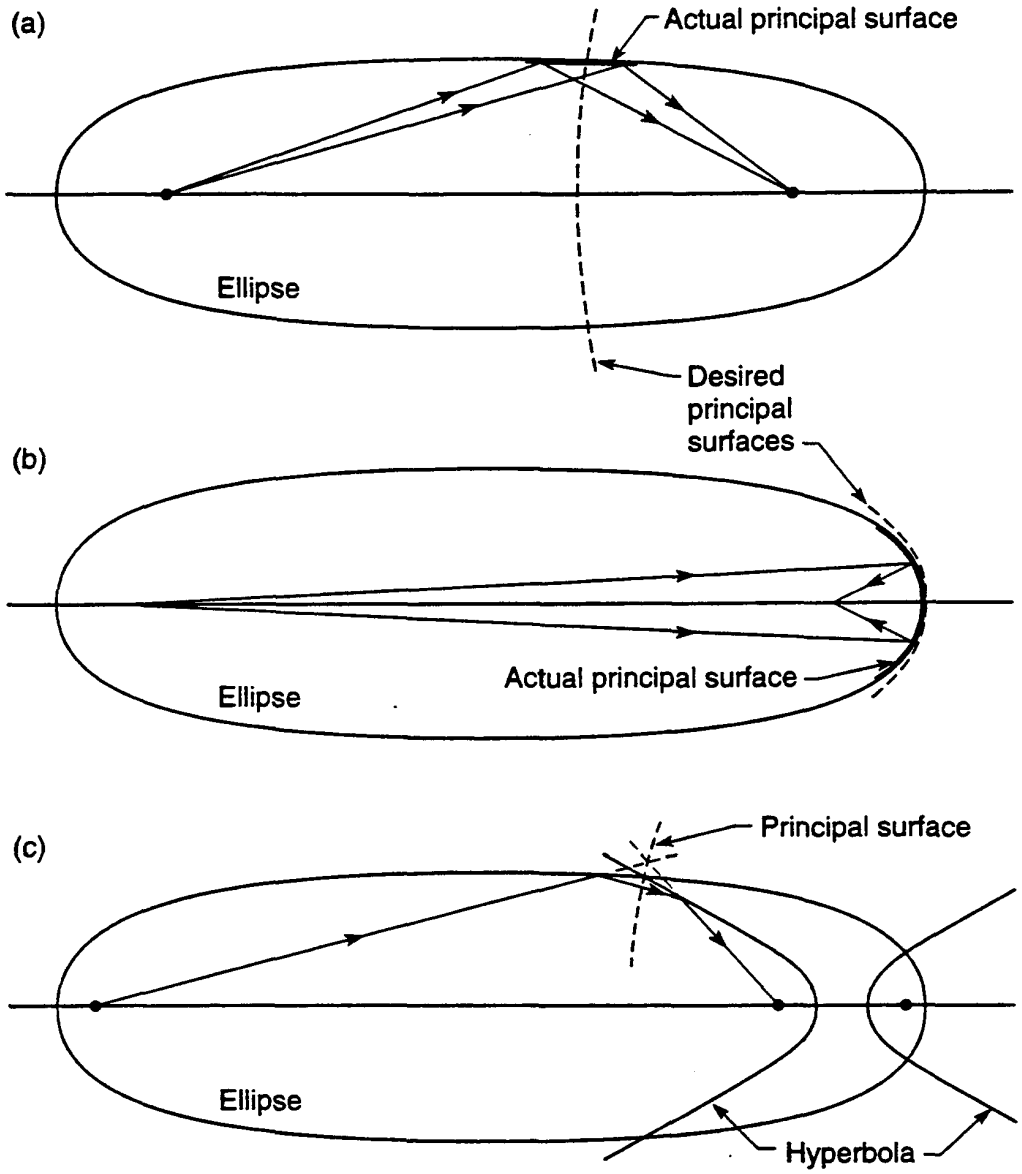

Figure 5. (a) Single-reflection imaging geometry in which the principal surface is the mirror itself, which is roughly perpendicular to the principal surface (shown dashed) needed to satisfy the sine condition. (b) Another single-reflection geometry but now at near normal incidence; the mirror and the desired principal surface almost coincide and thus lead to much higher quality imaging. (c) Double-reflection Wolter system in which the principal surface is a much better approximation to the desired surface than in (a).

$$R_c = \frac{r'\delta}{2}\left(\frac{1+\cos\psi}{\cos\psi}\right) \quad . \tag{27}$$

This has been an approximate treatment (Howells, 1980). Wolter's more accurate one reveals that the radius of the circle is actually given by

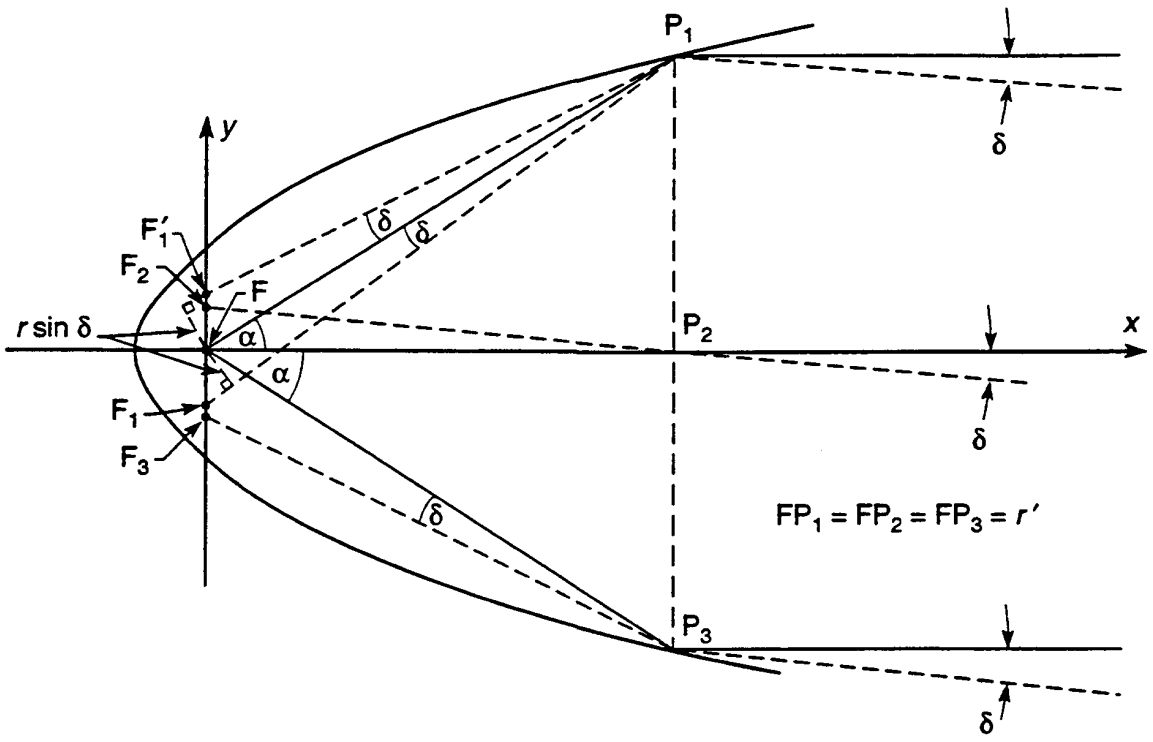

Figure 6. Definition of the points F, F_1, F_1', F_2, F_3 used in explaining the origin of coma in the single-reflection, grazing-incidence mirror with a symmetry axis.

$$R_c = \frac{r' \tan\delta}{2}\left(\frac{1+\cos\psi}{\cos\psi}\right) , \tag{28}$$

and that the center is shifted off axis by s where

$$s = -\frac{r' \tan\delta}{2}\left(\frac{1-\cos\psi}{\cos\psi}\right) . \tag{29}$$

Now consider a grazing-incidence ellipse in the same geometry but with the object point at a finite distance r from $P_1P_2P_3$ and displaced a distance Δ from the axis so that $\delta = \Delta/r$. Since ψ is small for grazing-incidence systems, we have $(1 + \cos\psi)/\cos\psi \approx 2$. Consequently, $R_c \approx (r'/r)\Delta$ or Δ times the magnification. Moreover, $(1 - \cos\psi)/\cos\psi \approx 0$ so $s \approx 0$. The conclusion is that *the image of an off-axis point is a circle centered on the axis with a radius such as to pass through the paraxial image point.*

That this aberration is really Seidel coma can be seen from the fact that it varies linearly with the field angle δ and also because each circular zone of the aperture contributes a circular aberration figure in the focal plane. Furthermore, each time the reflecting point runs once round the ring $P_1P_2P_3$, the ray traces out the circle *twice*, which is again characteristic of coma (Welford, 1962).

It is also clear from the above treatment that the normal-incidence conic has the expected well-corrected coma. For this case, the value of ψ is roughly 180° leading to $(1 + \cos\psi)/\cos\psi \approx 0$.

With this insight into the dominant field-angle-dependent aberration of the single grazing-incidence mirror, we can understand the well-known "bow-tie" shaped image that used to be troublesome at synchrotron radiation facilities before low-emittance electron beams became widespread. Consider a unity-magnification mirror comprising a segment of an ellipsoid of revolution that subtends a maximum angle Ω at the axis. The image of an off-axis point will be an arc of the image circle of angle 2Ω passing through the paraxial image of the object point. When the object is extended in one direction much more than the other, as synchrotron radiation sources often are, the result is a "bow-tie" image as explained in Fig. 7. Note that this behavior also follows the theory closely for a unity-magnification toroid, which *does* have a type of symmetry axis with the center points of the object and image lying on it. However, as the magnification departs from unity, the behavior initially continues roughly similarly, but the symmetry of the system has been broken and the aberrations are no longer strictly Seidel coma. Although there is no sudden change, the behavior becomes significantly different for magnifications far from unity.

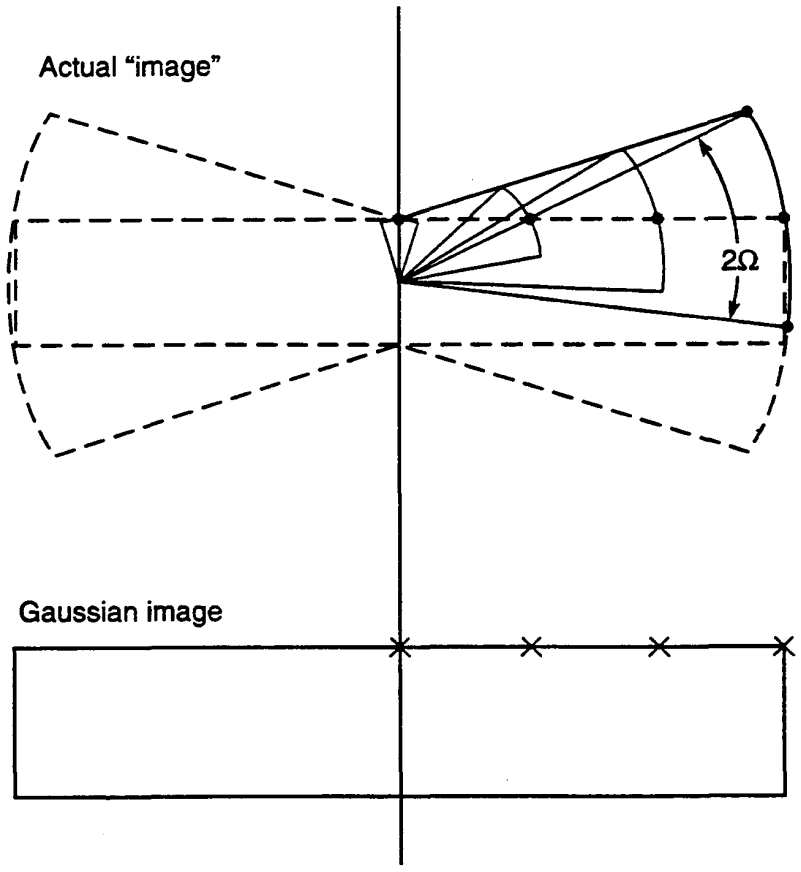

Figure 7. Explanation of how coma leads to a "bow-tie" image when a mirror with an axisymmetric (or nearly axisymmetric) shape is implemented over a segment of angular width $\Omega = 16.5°$.

9. Mirror Pairs in Wolter Geometry

We now return to the analysis of the focusing system shown in Fig. 6 with a view to elucidating the principle of the Wolter double-reflection system. Suppose that the ring $P_1P_2P_3$ contains the joint between the two reflectors and imagine the rays to be reflected twice, just in front of and just behind the joint. Considering the same three rays, we find that P_2F_2 behaves as before, while the rays through P_1 and P_3 are now deflected upward by δ instead of downward and arrive at F_1' as shown in Fig. 6. The rays through P_1 and P_3 now have

$$y = +\frac{r'\delta}{\cos\psi} \quad , \tag{30}$$

while the ray through P_2 continues to have $y \approx r'\delta$, so that the aberration circle, in the case of a Wolter system, has a radius R_w given by

$$R_w = \frac{r'\delta}{2}\left(\frac{1-\cos\psi}{\cos\psi}\right) \quad . \tag{31}$$

Equation (31) for R_w has the factor $(1-\cos\psi)/\cos\psi \approx 0$ for a grazing-incidence system, whereas the corresponding factor in Eq. (28) for R_c was approximately equal to 2. Thus the introduction of the double reflection brings about a large reduction in the aberration and allows one to design grazing-incidence systems with image quality similar to that of the normal-incidence conic. This is in accord with expectations based on the sine condition and the principal surface for the double-reflection system as shown in Fig. 5.

Although this discussion of the Wolter double-reflection principle contributes to our understanding of grazing-incidence mirror systems, it does not provide a blueprint for a new generation of improved beamline mirrors. The kind of high-quality image provided by a Wolter system is useful in imaging systems such as x-ray telescopes and may eventually be useful in x-ray microscopes. However, beamline mirrors are generally condensers and the fact that detail features *within* the object (which is usually the synchrotron source or a slit) are not accurately reproduced in the image is unimportant provided the overall *size* of the image is not significantly enlarged. The only useful improvement one would get by using a Wolter system as a condenser would be to eliminate the bow-tie effect, but as Fig. 7 shows, the gain in the flux that could pass through a slit would hardly make up for the losses of the mirror itself and would scarcely repay the investment needed for an extra aspheric mirror and all its accompanying systems.

One might ask whether there could be a role for the Wolter system as a collimating or focusing system for a monochromator. This is a different case and the higher-quality "lens" would have certain advantages. For example, even a perfect paraboloid mixes the horizontal and vertical divergences of the beam from a bending magnet, and this is a disadvantage in illuminating crystal monochromators which could probably be avoided by using the Wolter system. However, even when such advantages are taken into account, it is hard to imagine the high cost of a Wolter system of sufficient optical quality being considered acceptable for a beamline component. Moreover, the aberrations of focusing and collimating optics in grating monochromators must be combined with those of the grating, and the use of a better "lens" is an oversimplification of what is needed. The conclusion is that Wolter optics probably do not have a role in beamline systems for the time being. This is not to say that mirror pairs in general are not useful. Indeed, there are already several examples existing and proposed, and we can understand their operation in terms of the principles described above.

10. Mirror Pairs in General

There have been several studies carried out to identify the best way to combine the action of two mirrors or a mirror and a grating (Pouey, 1981, 1983; Aspnes, 1982; Hunter, 1981; Chrisp, 1983). Figure 8 shows several configurations involving two identical toroids, some of which tend to obey the sine condition (ϕ' increases when ϕ increases). Others radically disobey it (ϕ' decreases when ϕ increases). The dominant point aberrations F_{300} or F_{120} will not be improved by obeying the sine condition, but they can still be made to cancel. We will analyze this possibility in terms of wave-front errors. Even for the field aberrations, we expect a high degree of correction to be achieved only if there is an exact or approximate symmetry axis and the sine condition has an exact meaning. First consider the toroid in Fig. 8a and take F_{300} as an example. Based on the fact that the circular curvature of the mirror is too weak on the upstream side and too strong on the downstream (compared to the ideal paraboloid), we would expect the wave front emerging from the first mirror to be

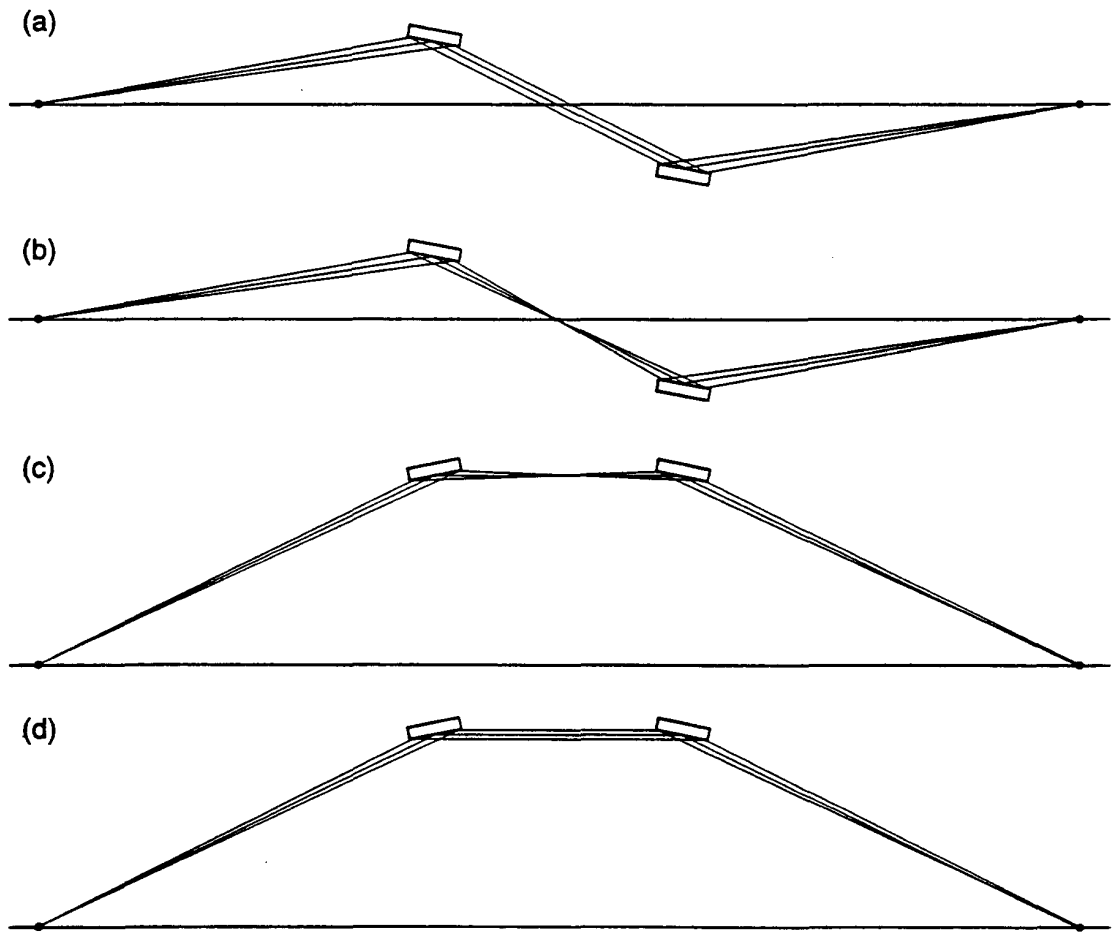

Figure 8. Four possible ways of combining two toroidal mirrors in pairs: (a) and (c) violate the sine condition grossly because the angle to the axis decreases at the outgoing side when it increases on the ingoing side; (b) and (d) satisfy the sine condition in this sense. On the other hand, (a) and (c) are configured for approximate cancellation of point aberrations depending on an odd power of w (aperture defect and line curvature), while (b) and (d) are not.

twisted, as described earlier, by an amount proportional to w^3 and to be leading the reference sphere above the principal ray and lagging it below. If we apply the same argument to the second mirror, we see that wave-front errors of opposite sign will be introduced by the second reflection, provided its direction is as shown in Fig. 8a. Note that this is the direction that strongly *disobeys* the sine condition. Similar arguments show that the wave-front errors corresponding to line curvature (which also depends on an odd power of w) will also be self-canceling for the same mirror configuration (Fig. 8a). That the configuration in Fig. 8a indeed gives a better image of the axial point than the inverse configuration (shown in Fig 8b) can be verified by ray tracing for particular geometries. It is noteworthy that these types of arguments depend on the aberrations being small enough and the mirrors close enough together that each ray is reflected at aperture coordinates (w, l) with substantially the same magnitudes (although maybe not the same signs) in each mirror. This is a condition that may not be met in real beamlines.

There are some similar comparisons between pairs of mirrors that do and do not obey the sine condition reported by Aspnes (1982) and Hunter (1981). One has to be careful in interpreting the results given by Aspnes because the toroids used had magnification values limited to unity or infinity. The choice of unity has special consequences because the point aberrations, line curvature and aperture defect, which would normally be dominant, happen to vanish at that value. As we have seen, the point and field aberrations must be considered separately and their relative importance depends on the source size and aperture size. Roughly speaking, the worst that can happen due to a field aberration is an extreme bow-tie effect that enlarges the short dimension of the synchrotron source or slit to equal the long one. On the other hand, the potential damage due to point aberrations is unlimited. For the small source sizes of modern storage rings, the best system design for a condenser will normally be one that corrects the point aberrations.

This discussion does not exhaust the possibilities of two-mirror systems. Readers wishing to explore further can refer to the paper by Namioka *et al.* (1983).

One can obviously design mirror pairs analogous to those in Fig. 8 using conics. Naturally these have no point aberrations, whichever way round they are, since they are the ideal point-imaging surfaces. However, it is important to recognize that manufacturing tolerances are likely to be larger for a conic than a toroid and will often more than outweigh the aberration advantage of conics.

Acknowledgements

This work was supported by the Director, Office of Energy Research, Office of Basic Energy Sciences, of the U.S. Department of Energy, under contract DE-AC03-76SF00098.

Appendix. The Optical Path Function Expansion for Gratings and Mirrors

According to Noda *et al.* (1974), the diffraction-grating optical, path function is given by

$$F = wF_{100} + wF_{102} + lF_{011} + \frac{1}{2}w^2F_{200} + \frac{1}{2}l^2F_{020} + \frac{1}{2}w^3F_{300} + \frac{1}{2}wl^2F_{120} + wlF_{111} + \frac{1}{8}w^4F_{400} + \frac{1}{4}w^2l^2F_{220} + \frac{1}{8}l^4F_{040} + \frac{1}{4}w^2F_{202} + \frac{1}{4}l^2F_{022} + \frac{1}{2}l^3F_{031} + \frac{1}{2}w^2lF_{211} + \ldots \quad . \tag{A1}$$

We have included the 102 term explicitly, whereas Noda *et al.* included it implicitly in the 100 term. F is the actual path length AB, and w and l are defined in Fig. A1. In F_{ijk}, i, j, and k are the powers of w, l, and z (or z') in the series expansion of F, each term of which represents a particular geometrical optical aberration. The terms go up to fourth order ($i + j + k \leq 4$) and are exactly those given by Noda *et al.* Those that have $j + k =$ odd have been omitted, being equal to zero by symmetry, and terms that have $i = j = 0$ are omitted because they do not represent aberrations. For the study of mirrors, we can use a still more restricted subgroup of the expressions for the F_{ijk}'s. First we reject the parts that represent the possibility that the grating is a holographic recording. This leads to

$$F_{ijk} = E_{ijk}(\alpha, r, z) + E_{ijk}(\beta, r', z') \quad , \tag{A2}$$

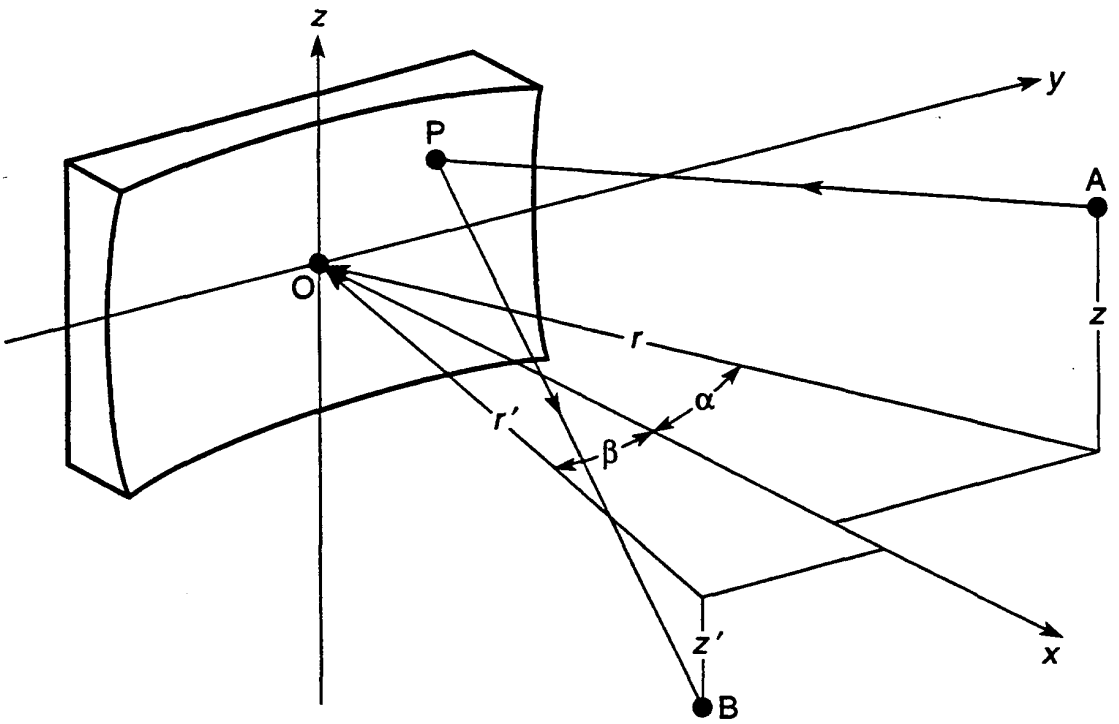

Figure A1. Coordinate system used discuss the optical path function analysis (after Noda, 1974).

where E_{ijk} is the expression given in Table A1. For a beamline mirror, it is often sufficient to consider a point source located in the symmetry plane of the mirror. This means $z = z' = 0$, $k = 0$. We also know that from the law of reflection that $\beta = -\alpha$, so that (A2) becomes

$$F_{ij0} = E_{ij0}(\alpha, r, 0) + E_{ij0}(-\alpha, r', 0) \quad . \tag{A3}$$

The function $E_{ij0}(\alpha, r, 0)$ is therefore tabulated in Table A-1, which uses the notations

$$T = \frac{\cos^2\alpha}{r} - 2a_{20}\cos\alpha \qquad S = \frac{1}{r} - 2a_{02}\cos\alpha \quad . \tag{A4}$$

S' and T' are also defined and are the same as S and T except that r is replaced by r'. The a_{ij} parameters have been discussed in detail for some important surfaces in the main text.

The terms in Eq. (A1) have some similarities with the terms in the aberration expansion of an axisymmetric optical system. The aperture coordinates w and l, for example, are basically the same as the aperture coordinates of an axisymmetric system. However, since our system has only a plane of symmetry rather than an axis, the notion of field coordinates is completely different. In fact, the conventional field angle or field coordinate, which would be measured from the axis, no longer exists in the absence of an axis and so aberrations that depend on it, such as Seidel coma, have no analog in the present study. One should not make the mistake of regarding z or z' as directly analogous to the "axisymmetric" type of field

TABLE A1. Values of $E_{ij0}(\alpha,r,0)$.

i \ j	0	1	2	3	4
0	0	0	S	0	$\frac{4a_{02}^2 - S^2}{r} - 8a_{04}\cos\alpha$
1	$-\sin\alpha$	0	$\frac{S\sin\alpha}{r} - 2a_{12}\cos\alpha$	0	*
2	T	0	$\frac{4a_{20}a_{02} - TS - 2a_{12}\sin 2\alpha}{r} + \frac{2S\sin^2\alpha}{r^2} - 4a_{22}\cos\alpha$	0	*
3	$\frac{T\sin\alpha}{r} - 2a_{30}\cos\alpha$	0	*	0	*
4	$\frac{4a_{20}^2 - T^2 - 4a_{30}\sin 2\alpha}{r} + \frac{4T\sin^2\alpha}{r^2} - 8a_{40}\cos\alpha$	0	*	0	*

coordinate. To see the error of this, consider the case in which both types of system are specialized to two dimensions so that only their tangential planes are considered. The axisymmetrical system still has a field coordinate measured from the axis, but for the plane-symmetric system, the restriction to the tangential (symmetry) plane implies $z = z' = 0$! The same error might lead us to look in Eq. (A1) for terms like w^3z or wl^2z to find the coma terms. But these terms are both symmetry-forbidden. There is no coma in the usual sense, and none of our coordinates w, l, or z (or z') can be identified as a conventional field coordinate.

In light of the above, it is perhaps unfortunate that a tradition has grown up in the synchrotron-radiation community of giving traditional names to the aberration terms in Eq. (A1) based on only partial similarities to the corresponding aberrations of the axisymmetric system. For example, the F_{120} and F_{300} aberrations, which have the same dependence on the *aperture* coordinates as conventional coma, have been referred to as "coma," even though there could be no similarity in their dependence on the *field* coordinates, as explained above. The present author has been among those guilty of this. It has been pointed out by Underwood (1992) that this can lead to important errors in the treatment of coma (see the section on the sine condition). Therefore we propose to continue to use traditional names only when the analogy is fairly complete. The following system of names is proposed:

F_{100}	Grating equation
F_{102}	Line curvature
F_{011}	Law of reflection in the sagittal plane
F_{200}	Tangential defocus
F_{020}	Astigmatism (sagittal defocus)
F_{300}	Aperture defect
F_{120}	Line curvature
F_{111}	Line curvature
F_{400}	Spherical aberration
F_{220}	220 aberration
F_{040}	Higher-order astigmatism
F_{202}	202 aberration
F_{022}	022 aberration
F_{031}	031 aberration
F_{211}	211 aberration

Of course, the treatment given so far does not enable one to calculate the most interesting thing, which is the extent of degradation (blurring) of the image that will be caused by any particular aberration. We now proceed to address that issue in the geometrical optics approximation. For each term of the aberration series, we calculate the ray aberrations (displacements from the paraxial image point), which in our notation are known as $\Delta y'$ and $\Delta z'$:

$$\Delta y'_{ij0} = \frac{r'}{\cos\alpha}\left(\frac{\partial F}{\partial w}\right)_{ij0} , \tag{A5}$$

and

$$\Delta z'_{ij0} = r'\left(\frac{\partial F}{\partial l}\right)_{ij0} \quad .$$

The total ray aberration in the $\Delta y'$ ($\Delta z'$) direction is the algebraic sum of the $\Delta y'_{ij0}$'s ($\Delta z'_{ij0}$'s). This means that partial or total cancellation of aberrations (known as "aberration balancing" when done deliberately) is possible and is sometimes useful.

$$\Delta y' = \sum_{ij} \Delta y'_{ij0} \quad \text{and} \quad \Delta z' = \sum_{ij} \Delta z'_{ij0} \quad . \tag{A6}$$

Equations (A5) are central to the geometrical theory of aberrations. Proofs are provided, for example, by Welford (1962) and Born and Wolf (1980). Neither of these authors includes the case of grazing incidence, which differs from the standard case of axial symmetry by the factor $1/\cos\alpha$ in the first of Eqs. (A5). This arises simply from the coordinate change involved in rotating the exit pupil so that it can be perpendicular to the outgoing principal ray. For the slow systems involved in grazing-incidence optics, Eqs. (A5) give an excellent approximation. For very fast systems of f-1 and faster, more complex expressions are needed as provided, for example, by McKinney and Palmer (1987).

As an example of the application of Eqs. (A5) and (A6), we show some ray traces in Fig. A3. The rays traced are shown in Fig. A2 and are done in double precision, so all aberrations up to very high order are accurately represented. To illustrate the action of Eqs. (A5) in determining the pattern of ray intersections in the receiving plane, we try to explain the general features of the ray traces in terms of the lowest-order aberrations. In the general case, we approximate $\Delta x'$ and $\Delta y'$ as

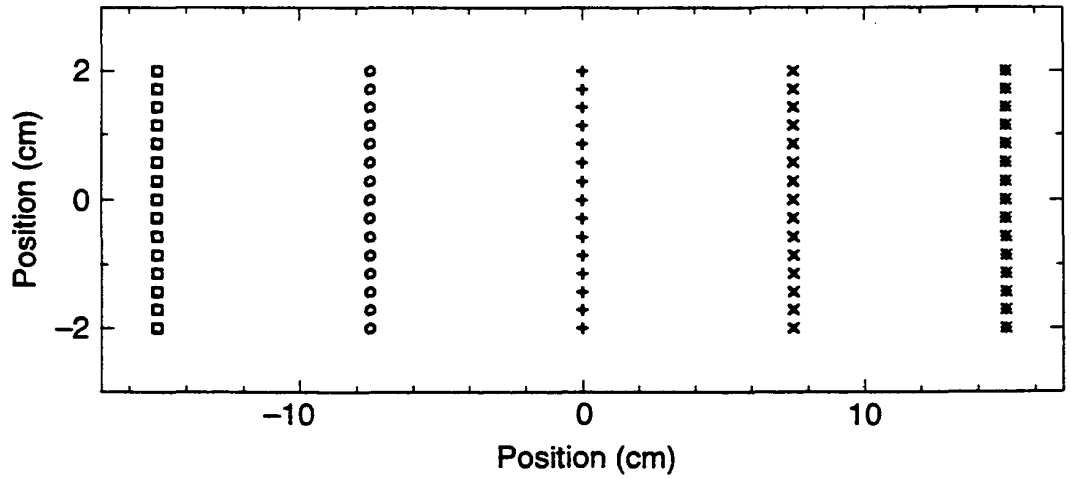

Figure A2. Layout of the 5 × 15 ray points and their plot labels used in the ray trace shown in Figure A3. This figure shows the pattern of intersections of the rays with the *tangent plane* at the pole of the toroidal mirror. The rays travel from left to right.

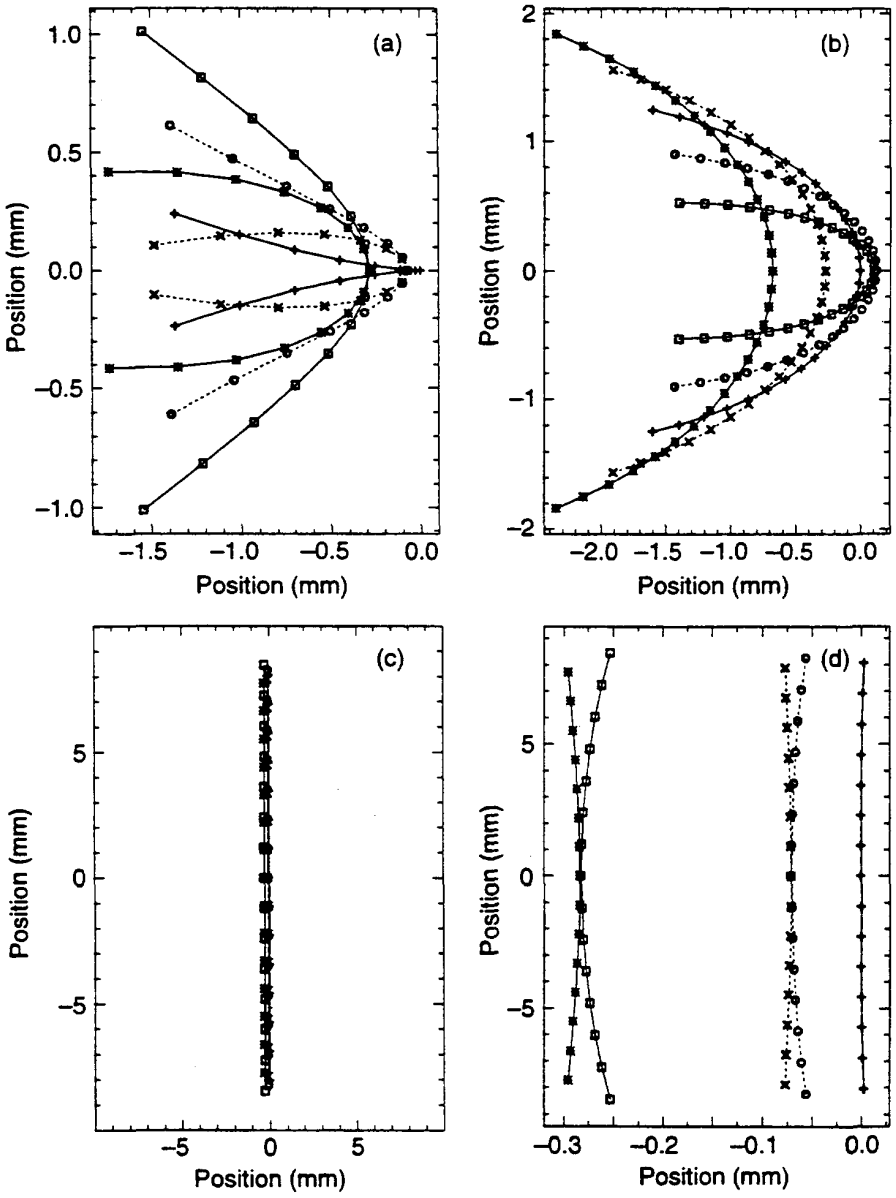

Figure A3. Ray traces of the images of a point source produced by a toroidal mirror under various conditions. The 5 × 15 pattern of incoming rays and their plot symbols are shown in Figure A2. The parameters of the system for the image shown in (a) are: $r = 10$ m, $r' = 2$ m, $\alpha = 88°$, $R = 95.55123612$ m, $\rho = 0.1163316560$ m. The mirror area (tangential × sagittal), measured in its tangent plane, is 300 × 40 mm^2. R and ρ are calculated to give a stigmatic image, and we follow the standard practice of using extreme precision for calculated numbers input to the ray-trace code. Figure (a) is the image in the focal plane for the above system. Figure (b) shows the image from the same system but in a plane 15 cm downstream of the focus and with a 5 × 31 ray pattern. In Figure (c) the system is the same as in (a) except that the value of ρ has been increased to the value (0.1744974840 m) given by Eq. (10) to demonstrate that the line image indeed becomes straight as predicted. Figure (d) is the same as (c) but with an expanded transverse scale so that the residual aberrations can be seen.

$$\Delta z' = r'\left[F_{020}l + F_{120}wl\right] \tag{A7}$$

and

$$\Delta y' = \frac{r'}{\cos\alpha}\left[\frac{1}{2}F_{120}l^2 + F_{200}w + \frac{3}{2}F_{300}w^2\right] . \tag{A8}$$

Notice we are ignoring the second and third terms in Eq. (6) in our representation of the line-curvature aberration. This is valid provided we are dealing with a steeply curved toroid ($\rho << R$). Substituting for l from (A7) into (A8) we get

$$\Delta y' = \frac{r'}{\cos\alpha}\left[F_{120}\frac{\Delta z'^2}{2r'^2\left(F_{020} + F_{120}w\right)^2} + F_{200}w + \frac{1}{2}F_{300}w^2\right] . \tag{A9}$$

Equation (A9) shows some of the characteristics we see in the ray traces. For example, when $F_{020} = F_{200} = 0$ representing a stigmatic focus, which is the condition prevailing in Fig. A3(a), Eq. (A9) predicts a family of parabolas, each with a semi-latus rectum that increases with increasing w and a $\Delta y'$-directed shift proportional to w^2. Most of these features can be seen in Fig. A3(a). On the other hand, when $F_{020} = w = 0$ (the plus signs in Fig. A2), Eq. (A7) predicts that $\Delta z' = 0$. The line traced out by the plus signs does show this behavior at low l, but at high l, some higher-order aberrations give an increase in $\Delta z'$. Study of the rate at which $\Delta z'$ increases with l (measured in plus-sign intervals) shows it to be an F_{040} effect, i.e., $\Delta z'$ proportional to l^3. Figure A3(b) shows more aberrations because now $F_{020}, F_{200} \neq 0$, but it continues to show, basically, a family of parabolas. In the symmetry plane ($l = \Delta z = 0$), we have two effects determining $\Delta y'$, a w effect (defocus) and a w^2 effect (aperture defect). Starting from the plus sign at (0, 0), we can see that the sizes and directions of the shifts along the $\Delta y'$ axis are intelligible on this basis. Turning to Fig. A3(c), we see a large astigmatism (long focal line) and no defocus, and we see clearly that application of Eq. (10) in choosing ρ correctly delivers a straight focal line. Examination of the expanded diagram in Fig. A3(d) reveals that the only horizontal shift along the $\Delta y'$ axis is the w^2 one (aperture defect), as it should be, since we are now in focus. Moreover, we see another aberration that gives a slight line curvature with equal sizes but opposite signs for positive and negative values of w: the hallmark of the F_{220} effect.

References

Abbe, E., "Ueber die Bedingungen des Aplanatismas der Linsensysteme," Sitz. Jenaisch. Ges. Med. Naturwissen **13** (Sitz. Ber. VIII-2), 129–142 (1879).

Aspnes, D.E., "Imaging Performance of Mirror Pairs for Grazing Incidence Applications: a Comparison," Appl. Opt. **21**, 2642–2646 (1982).

Beutler, H.G., "The Theory of the Concave Grating," J. Opt. Soc. Am. **35**, 311–350 (1945).

Born, M., and E. Wolf, *Principles of Optics* (Pergamon Press, Oxford, 1980).

Brueggemann, H.P., *Conic Mirrors* (Focal Press, London, 1968).

Chrisp, M.P., "Aberrations of Holographic Toroidal Grating Systems," Appl. Opt. **22**, 1508–1518 (1983).

Combleet, S., *Microwave and Optical Ray Geometry* (John Wiley, Chichester, 1984).

Haber, H., "The Torus Grating," *J. Opt. Soc. Am.* **40**, 153–165 (1950).

Hogrefe, H., M.R. Howells, and E. Hoyer, "Application of Spherical Gratings in Synchrotron Radiation Spectroscopy," Proc. SPIE **733**, 274–285 (1986).

Howells, M.R., "Beamline Design for Synchrotron Spectroscopy in the VUV," *Appl. Opt.*, **19**, 4027–4034 (1980).

Hunter, W.R., "Aberrations of Grazing Incidence Systems and Their Reduction or Toleration," Proc. SPIE, **315**, 19–29 (1981).

Kirkpatrick, P., and A.V. Baez, "Formation of Optical Images by X-Rays," J. Opt. Soc. Am. **38**, 776–774 (1948).

Korsch, D., *Reflective Optics* (Academic, Boston, 1991).

Longhurst, R.S., *Geometrical and Physical Optics* (Longmans, London, 1962).

McKinney, W.R., and C. Palmer, "Numerical Design Method for Aberration-Reduced Concave Grating Spectrometers," Appl. Opt. **26**, 3108–3018 (1987).

Namioka, T., "Design Studies of Mirror-Grating Systems for Use with an Electron Storage Ring Source at the Photon Factory," Nucl. Instrum. Methods **208**, 215–222 (1983).

Noda, H., T. Namioka, and M. Seya, "Geometrical Theory of the Grating," J. Opt. Soc. Am. **64**, 1031–10366 (1974).

Nyholm, R., S. Svenson, and J. Nordgren, "A Soft X-ray Monochromator for the MAX Synchrotron Facility," Nucl. Instrum. Methods **A246**, 267–271 (1986).

Petersen, H., "The Plane Grating and Elliptical Mirror: a New Optical Configuration for Monochromators," Opt. Commun. **40**, 402–406 (1982).

Pouey, M.R., M.R. Howells, and P.Z. Takacs, "Visible Ultra Violet Optical Design of Toroidal Mirror-Toroidal Grating Combinations," Proc. SPIE **315**, 37–43 (1981).

Pouey, M., Howells, M.R., and Takacs, P.Z., "Optical Design of Grazing Incidence Toroidal Grating Monochromator," Nucl. Instrum. Methods **195**, 223–232 (1983).

Rehn, V., "Optics for Insertion-Device Beamlines," Proc. SPIE **582**, 238–250 (1985).

Underwood, J., "X-ray Optics," American Scientist **66**, 476–486 (1978).

Underwood, J.H. (private communication, 1992).

Underwood, J.H., A.C. Thomson, Y. Wu, and R.D. Giauque, "X-ray Microprobe Using Multilayer Mirrors," Nucl. Instrum. Methods **A266**, 296–302 (1988).

Welford, W., "Aberration Theory of Gratings and Grating Mountings," *Progress in Optics*, edited by E. Wolf, **4**, 241–280 (1965).

Welford, W., "Aplanatism and Isoplanatism," *Progress in Optics*, edited by E. Wolf, **13**, 268–292 (1976).

Welford, W.A., *Geometrical Optics* (North Holland, Amsterdam, 1962).

Wolter, H., "Spiegelsystem Streifenden Einfalls als Abbildende Optiken für Röntgenstrahlen," Ann. Phys. **10**, 94–114 (1952).